

# Modeling the dynamic behaviors of the COPI vesicle formation regulators, the small GTPase Arf1 and its activating Sec7 guanine nucleotide exchange factor GBF1 on Golgi membranes

Garrett Sager<sup>a,b,t,\*</sup>, Tomasz Szul<sup>a</sup>, Eunjoo Lee<sup>a</sup>, Ryoichi Kawai<sup>b</sup>, John F. Presley<sup>c</sup>, and Elizabeth Sztul<sup>a</sup>

<sup>a</sup>Department of Cell, Developmental, and Integrative Biology and <sup>b</sup>Department of Physics, University of Alabama at Birmingham, Birmingham, AL 35294; <sup>c</sup>Department of Anatomy & Cell Biology, McGill University, Montreal, QC H3A 0C7, Canada

**ABSTRACT** The components and subprocesses underlying the formation of COPI-coated vesicles at the Golgi are well understood. The coating cascade is initiated after the small GTPase Arf1 is activated by the Sec7 domain-containing guanine nucleotide exchange factor GBF1 (Golgi brefeldin A resistant guanine nucleotide exchange factor 1). This causes a conformational shift within Arf1 that facilitates stable association of Arf1 with the membrane, a process required for subsequent recruitment of the COPI coat. Although we have atomic-level knowledge of Arf1 activation by Sec7 domain-containing GEFs, our understanding of the biophysical processes regulating Arf1 and GBF1 dynamics is limited. We used fluorescence recovery after photobleaching data and kinetic Monte Carlo simulation to assess the behavior of Arf1 and GBF1 during COPI vesicle formation in live cells. Our analyses suggest that Arf1 and GBF1 associate with Golgi membranes independently, with an excess of GBF1 relative to Arf1. Furthermore, the GBF1-mediated Arf1 activation is much faster than GBF1 cycling on/off the membrane, suggesting that GBF1 is regulated by processes other than its interactions Arf1. Interestingly, modeling the behavior of the catalytically inactive GBF1/E794K mutant stabilized on the membrane is inconsistent with the formation of a stable complex between it and an endogenous Arf1 and suggests that GBF1/E794K is stabilized on the membrane independently of complex formation.

## Monitoring Editor

Jennifer Lippincott-Schwartz  
Howard Hughes Medical  
Institute

Received: Sep 14, 2020

Revised: Dec 3, 2020

Accepted: Dec 29, 2020

## INTRODUCTION

Membrane traffic is an essential process in eukaryotic cells and is required to support such essential cellular activities as growth, compartment biogenesis and homeostasis, and sensing and responding

to extracellular stimuli. Key events in membrane traffic are supported by a multitude of highly conserved genes, and deletion or mutation of such genes often leads to cellular death, underscoring the importance of the process.

Membrane traffic within the secretory and endocytic pathways is mediated by vesicular carriers that form at the donor compartment, transit some distance through the cell, and then recognize and fuse with the acceptor membrane to deliver their cargo (Szul and Sztul, 2011; Wang *et al.*, 2017). Vesicular traffic is selective and requires a mechanism to specifically package only some proteins into the forming vesicle while excluding others (Derby and Gleeson, 2007; Dancourt and Barlowe, 2010; Lord *et al.*, 2013; Tan and Gleeson, 2019; VanWinkle *et al.*, 2020). Cargo protein selection is mediated by a generally conserved mechanism that involves the assembly of a coat lattice on the cytosolic face of the donor membrane that “holds” cargo proteins within a spatially defined patch that

This article was published online ahead of print in MBoC in Press (<http://www.molbiolcell.org/cgi/doi/10.1091/mbc.E20-09-0587>) on January 6, 2021.

<sup>†</sup>Present address: Biochemistry, Quantitative Biology, Biophysics, and Structural Biology Graduate Program, Yale University, New Haven, CT 06511.

\*Address correspondence to: Garrett Sager ([garrett.sager@yale.edu](mailto:garrett.sager@yale.edu)).

Abbreviations used: ARF1, ADP-ribosylation factor 1; FRAP, fluorescence recovery after photobleaching; GBF1, Golgi brefeldin A resistant guanine nucleotide exchange factor 1.

© 2021 Sager *et al.* This article is distributed by The American Society for Cell Biology under license from the author(s). Two months after publication it is available to the public under an Attribution–Noncommercial–Share Alike 3.0 Unported Creative Commons License (<http://creativecommons.org/licenses/by-nc-sa/3.0>).

“ASCB®,” “The American Society for Cell Biology®,” and “Molecular Biology of the Cell®” are registered trademarks of The American Society for Cell Biology.

subsequently invaginates to form a bud and ultimately pinches off as a vesicle. A family of structurally and functionally related coat complexes exist in cells to traffic proteins at different donor–acceptor membrane interfaces (Barlowe, 2000; Scales *et al.*, 2000; Gleeson *et al.*, 2004; Faini *et al.*, 2013; Dell’Angelica and Bonifacino, 2019). At the endoplasmic reticulum (ER)–Golgi interface, vesicles coated with components of the COPII coat transport newly synthesized proteins from the ER to the Golgi, while vesicles coated with COPI components appear to retrieve escaped and cycling proteins from the Golgi back to the ER (Kuehn and Schekman, 1997; Lowe and Kreis, 1998; Barlowe, 2000, 2002; Tang *et al.*, 2005; Stagg *et al.*, 2007; Miller and Barlowe, 2010; Szul and Sztul, 2011; D’Arcangelo *et al.*, 2013; Faini *et al.*, 2013; Arakel and Schwappach, 2018; Bethune and Wieland, 2018).

The molecular events generating COPI vesicles from Golgi membranes have been reconstituted *in vitro* in a process requiring the activated GTP-bound form of the small Ras-related GTPase Arf1 and the heptameric coatomer complex (Ostermann *et al.*, 1993; Rowe *et al.*, 1996; Spang *et al.*, 1998). Like all GTPases, Arf1 cycles between the activated GTP-bound conformation and the inactive GDP-bound conformation. Arf1 is posttranslationally modified through the attachment of the hydrophobic myristic acid at glycine in position 2 within its N-terminus, and this moiety is buried within the Arf1 while the protein is in the inactive GDP-bound form in the cytosol (Franco *et al.*, 1995, 1996; Goldberg, 1998). To become activated, Arf1 must associate with a membrane and then be a substrate for an enzyme, a guanine nucleotide exchange factor (GEF) that facilitates the expulsion of the GDP and allows the binding of the activating GTP to the Arf.

Mammalian cells contain 15 Arf GEFs characterized by a highly conserved catalytic Sec7 domain, initially identified in the Sec7p protein of the yeast *Saccharomyces cerevisiae* (Bussey *et al.*, 1983; Goldberg, 1998; Casanova, 2007; Bui *et al.*, 2009; D’Souza and Casanova, 2016; Sztul *et al.*, 2019). The GEF required for Arf1 activation that leads to the formation of COPI vesicles has been identified as GBF1 (Golgi brefeldin A resistant guanine nucleotide exchange factor 1), a GEF belonging to the GBF1/BIG superfamily (Claude *et al.*, 1999; Kawamoto *et al.*, 2002; Garcia-Mata *et al.*, 2003; Szul *et al.*, 2005, 2007; Zhao *et al.*, 2006; Wright *et al.*, 2014).

GBF1-catalyzed GDP/GTP exchange on Arf1 causes a conformational switch within Arf1 that exposes the hydrophobic myristic acid and allows its stable insertion into the membrane, securing the active Arf1-GTP on the lipid bilayer. Because of the allosteric coordination between the GDP/GTP exchange and myristic acid insertion, Arf1 activation can occur exclusively on the membrane. Furthermore, the insertion of the myristic acid is simultaneous with the alignment of the N-terminal  $\alpha$ -helix of Arf1 onto the membrane, and the two processes confine Arf1 within a sterically restricted conformation on the membrane that exposes the effector-interacting interface (Nawrotek *et al.*, 2016). The active Arf1-GTP then recruits cytosolic coatomer, but the exact stoichiometry of Arf1-coatomer binding is unclear, as multiple subunits of coatomer ( $\beta$ ,  $\gamma$ ,  $\Delta$ , and  $\epsilon$ ) contain Arf-binding sites (Szul and Sztul, 2011). Experimental evidence suggests that two Arf1 molecules, separated by 110 Å, bind per coatomer (Yu *et al.*, 2012). Repeated cycles of GBF1-mediated Arf1 activation and coatomer binding, combined with the recruitment of accessory proteins, ultimately result in COPI vesicle formation.

Extensive enzymatic, biochemical, and molecular analyses combined with crystallography, cryogenic electron microscopy-EM, and other structural approaches, provided an in-depth understanding of how the Sec7 domains of GEFs mediate the Arf1-activating GDP/GTP exchange (Beraud-Dufour *et al.*, 1998; Cherfils *et al.*, 1998;

Renault *et al.*, 2002). However, we still are largely ignorant of how Arf1 and GBF1 diffuse within the cytosol to approach Golgi membranes, how they associate with Golgi membranes through transient and stable interactions, and how they interact with each other and with other components once on the membrane. We also lack an even basic understanding of how such interactions impact the overall dynamics of the coating process. For example, GBF1 may have multiple roles during COPI coating, and in addition to binding and activating Arf1 to initiate the coating cascade, GBF1 also binds the coatomer (Deng *et al.*, 2009), perhaps “helping” Arf1 to recruit the coat.

To determine the parameters and relationships between Arf1 and GBF1 behavior on Golgi membranes in live cells, we used fluorescence recovery after photobleaching (FRAP) and computational simulations under conditions where distinct subprocesses of Arf1 activation and/or coating were perturbed by molecular means. Significantly, while previous studies reported the FRAP of Arf1 and GBF1 (and mutants of each protein) when each protein was expressed individually in cells, we performed dual FRAP in cells coexpressing both proteins and imaged simultaneously. Importantly, a comparison of single versus dual FRAPs shows a significant change in qualitative behavior of Arf1, but not GBF1. Our results suggest that Arf1 and GBF1 associate with Golgi membranes independently of each other and that Arf1 dynamics are limited by reaction rate, while GBF1 is solely diffusion limited.

Our results also have more general implications for the way FRAP data are analyzed, especially when protein dynamics are measured during transient overexpression. Historically, the  $t_{1/2}$  has been used as the most popular metric to summarize FRAP data and to compare FRAPs of different proteins. However, we now show that plotting FRAP data on a semi-log plot can highlight the qualitative features (diffusion or reaction[s]) that are most important for regulating a specific protein’s intracellular dynamics. Importantly, we also show that these qualitative features can be obscured when proteins are overexpressed in cells, suggesting that some phenotypes observed by studying the behavior of a single expressed protein may be an artificial result of altering qualitative protein dynamics. Additionally, we document that studying the kinetic behavior of a protein coexpressed with a mutant reaction partner can lead to complex dynamics due to the ability of the protein to interact with both, the mutant reaction partner as well as the endogenous wild-type protein.

## RESULTS

### Coating subprocesses

We aim to describe the parameters of Arf1 and GBF1 behavior on Golgi membranes during COPI vesicle formation. The overall coating process and the association/dissociation events that we are monitoring by FRAP and simulating are shown in Figure 1. In our model, Arf1-GDP and GBF1 arrive separately at Golgi membranes. Arf1-GDP has been proposed to bind to the SNARE membrane in a GTP-independent manner before interacting with GBF1 (Honda *et al.*, 2005). Arf1 and GBF1 subsequently form a complex (step 1), followed by the exchange of GTP for GDP and the insertion of Arf1 into the membrane (step 2). Arf1-GTP then separates from GBF1 while maintaining membrane association (step 3). Finally, Arf1-GTP forms a complex with coat and with GAP (step 4). Continuous formation of such complexes will ultimately lead to vesicle formation and its budding from Golgi membranes (Peter *et al.*, 1993; Scales *et al.*, 1997; Shima *et al.*, 1999). To simplify the modeling scope, only Arf1 and GBF1 are explicitly considered, and all other reactions needed to form a vesicle are considered as one transition rate.

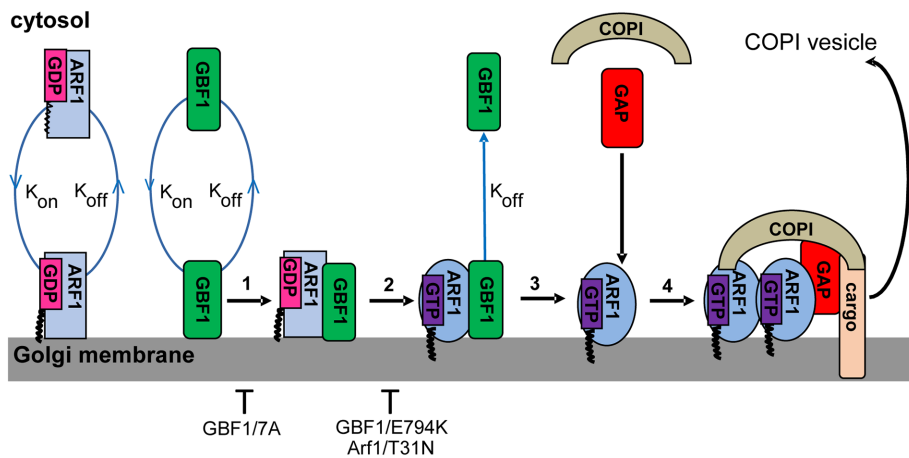


**FIGURE 1:** Subprocesses of COPI vesicle formation. Schematic of the four steps leading to Arf1 activation by GBF1 and the association/dissociation constants relevant for developing simulations for the dynamics of Arf1 and GBF1 during coating. Initially, Arf1-GDP and GBF1 are associating and dissociating with the membrane with rate constants  $k_{on}$  and  $k_{off}$ , respectively. GBF1 activates Arf1 by GDP/GTP exchange, which leads to a molecular cascade that forms a COPI vesicle.

To refine our models, we used molecular approaches to selectively perturb specific subprocesses through the expression of dominant inactive mutants of Arf1 and GBF1 (labeled underneath the membrane in Figure 1) and assess the effect of such changes on the FRAP of each protein. The contribution of the initial interaction of Arf1 with GBF1 to their membrane dynamics was probed by assessing the behavior of the GBF1/7A mutant and the behavior of Arf1 in cells expressing this mutant (Figure 1, step 1). The GBF1/7A mutant contains a mutation in a loop after helix J within its Sec7 domain, and although this GBF1 mutant associates with Golgi membranes, it is incapable of binding Arf1 (Lowery *et al.*, 2011). When expressed in cells, GBF1/7A causes Golgi disruption, presumably by competing with the endogenous GBF1 for Golgi binding sites, thus preventing the activation of the endogenous Arf1. The importance of the next step, GDP expulsion from Arf1 by GBF1, to their dynamics was probed by examining the FRAP of the GBF1/E794K mutant and the behavior of Arf1 in cells expressing this mutant (Figure 1, step 2). GBF1/E794K was shown to associate with Golgi membranes and to bind Arf1, but is incapable of sterically displacing GDP from Arf1 (Garcia-Mata *et al.*, 2003; Szul *et al.*, 2005; Bouvet *et al.*, 2013). The GBF1/E794K mutant also causes Golgi disruption, either by competing with the endogenous GBF1 for Golgi binding sites or by competing for the Arf1 substrate, in both cases preventing Arf1 activation. We also perturbed the coating process by expressing the Arf1/T31N mutant previously shown to have low affinity for both GDP and GTP (Peters *et al.*, 1995). Although we tentatively place its inhibitory action at step 2, it remains possible that Arf1/T31N does not stably associate with GBF1 (as explored below). In all cases, we measured the FRAP of each protein when coexpressed with a cognate partner listed in Supplemental Table 1.

### Theoretical correlation between FRAP and reaction-diffusion kinetics

From a theoretical perspective, the exchange of a bleached protein or a protein complex on the Golgi membrane measured by FRAP is generally either diffusion limited (restricted by how fast the protein diffuses in the cytosol and on the membrane) or reaction limited (regulated by how fast the protein associates/dissociates

with the membrane and reacts with the relevant substrate or enzyme) (Sprague *et al.*, 2004). Diffusion-limited FRAP was the earliest analyzed case, and the solution for the diffusion constant,  $D$ , is well characterized:

$$D = 0.224 \frac{r^2}{t_{1/2}} \quad (1)$$

where the diffusion constant can be calculated by knowing only the time it takes for the photobleached region of interest (ROI) to reach half of its final intensity,  $t_{1/2}$ , and the radius,  $r$ , of the bleached ROI (Peters *et al.*, 1974; Poo and Cone, 1974; Axelrod *et al.*, 1976; Edidin *et al.*, 1976; Jacobson *et al.*, 1976; Schlessinger *et al.*, 1976; Zagayansky and Edidin, 1976). The  $t_{1/2}$  is a frequently used method to summarize FRAP data and allows direct comparisons of FRAPs for multiple components within a single process (Nehls *et al.*, 2000; Kuhn *et al.*, 2011). These comparisons are generally interpreted as reflecting how fast or slow a protein recovers

and suggest which proteins may be “held back” by some additional process.

Most relevant for reaction-limited FRAP data analysis is the effect of protein overexpression on reaction rates via the law of mass action. Conceptually, it is well agreed that overexpression can affect cellular dynamics through multiple mechanisms such as resource overload, stoichiometric imbalances, promiscuous interactions, and pathway modulation (Moriya, 2015). Resource overload occurs when the overexpressed protein requires resources that are needed by other pathways. For instance, if the protein uses chaperones, the overexpressed protein may be taking away chaperones needed to fold proteins required for a basic cellular function. Stoichiometric imbalance happens when a single subunit of a hetero-oligomer is overexpressed, which can cause an abnormal, toxic protein complex (Abruzzi *et al.*, 2002). Promiscuous interactions occur if an overexpressed protein contains a highly unstable, flexible region, because such domains can interact with low affinities with numerous proteins, leading to unpredictable consequences. Pathway modulation ensues when regulatory proteins are overexpressed, which may increase essential reaction rates and change the qualitative behavior of a pathway. While each of these four perturbation mechanisms seems conceptually probable, there is a lack of quantitative data assessing how much overexpression can change the qualitative interpretation of kinetic experiments. Here, we address this gap by using FRAP as a model kinetic experiment and the behavior of Arf1 and GBF1 during COPI vesicle formation at the Golgi as a model biological system.

Mathematically, determining whether a process is reaction or diffusion limited from FRAP data can be fairly simple. For a normalized FRAP curve of  $I(t)$  (intensity at time  $t$ ), it can be achieved by plotting the inverse intensity,  $K(t) = 100 - I(t)$  (100 is used because the FRAP data are normalized to 100). When the recovery is limited by one, first-order reaction,  $K(t)$  can be fitted with a single exponential:

$$K(t) = K_0 e^{-kt} \quad (2)$$

where  $K_0$  is 100 minus the mean intensity in the ROI in the frame immediately after the bleach and  $k$  is the reaction rate. Taking the natural logarithm of Eq. 1 yields

GBF1 environment	$t_{1/2}$	Limiting process	Arf1 environment	$t_{1/2}$	Limiting process
GBF1 WT (without Arf1 coexpression)	7.5	Diffusion	Arf1 WT (without GBF1 coexpression)	10.3	Two reactions
GBF1 WT (with Arf1 coexpression)	4.5	Diffusion	Arf1 WT (with GBF1 WT coexpression)	12.3	One reaction
GBF1 WT (with Arf1/T31N coexpression)	6.7	Diffusion	Arf1 T31N (with GBF1 WT coexpression)	2.9	Diffusion
GBF1/E794K (with Arf1 WT coexpression)	19.7	One reaction	Arf1 WT (with GBF1 E794K coexpression)	7.2	Diffusion
GBF1/7A (with Arf1 WT coexpression)	5.2	Diffusion	Arf1 WT (with GBF1 7A coexpression)	7.6	Two reactions

Mean  $t_{1/2}$  values for GFP-tagged GBF1 constructs expressed alone or coexpressed with Arf1-mCherry constructs and for Arf1-mCherry alone or coexpressed with GFP-tagged GBF1 constructs. The SD and statistical significance for these measurements are presented in Supplemental Tables 2 and 3.

**TABLE 1:** GBF1 and Arf1 FRAP  $t_{1/2}$  and limiting process under different conditions.

$$\ln[K(t)] = -kt + \ln[K_0] \quad (3)$$

Comparing Eq. 3 to the linear equation,  $y = mx + b$ , shows that the slope of Eq. 3 is  $-k$ . Plotting a hypothetical FRAP limited by one, first-order reaction, as mathematically represented by Eq. 2, on a semi-log plot effectively takes Eq. 2 and makes the function appear as Eq. 3. Therefore, the slope of the line on the semi-log plot is proportional to the negative reaction rate (Figure 2A). The more “downward” the line, the faster the reaction. FRAP data represented by a simple exponential decay indicate that the recovery is limited by a single rate process, such as on-off exchange between cytosol and membrane or a single reaction with another macromolecule. Diffusion is so fast that it is invisible in the hypothetical recovery curve.

When FRAP is limited by multiple first-order reactions, the data can be fitted by a linear combination of exponentials (Figure 2B). In this example, a fast reaction dominates the dynamics for the initial part of the recovery (about the first 25 s), until the slower reaction limits the dynamics for the latter portion. In this scenario, when  $K(t)$  is graphed on a semi-log plot, the curve can be fitted by two straight lines. Unfortunately, it is difficult to visually differentiate between FRAP data limited by multiple reactions or diffusion (described

below). In such cases, other information can help to make an educated prediction about whether the dynamic behavior of a protein is limited by multiple reactions or is diffusion limited. For example, knowing that a molecule has a small diffusion constant would suggest that its dynamics are likely limited by diffusion.

Another issue that can arise during FRAP analysis, especially when multiple reactions limit the protein’s kinetics, is the temporal resolution of the data. There is a trade-off between sampling with high temporal resolution for a short time and sampling with lower temporal resolution for longer time. For the semi-log method, we decided to use the former strategy. From past reports monitoring the recovery of COPI coat components over 2 or 3 min, it was observed that not much additional recovery occurs after 60 s, so there is little information to be gathered in the latter portion of the recovery curve (Niu *et al.*, 2005; Szul *et al.*, 2005; Bhatt *et al.*, 2016). The first 30–40 s seems to be the richest in information. Thus, it is more advantageous to more densely sample the system for the first 40–60 s than was done in previous reports. For instance, it is common for FRAP reports to measure the sample every 4–5 s. We chose to employ a higher sampling rate to allow detecting processes with shorter timescales.

The other common limiting process during FRAP is diffusion. In this scenario,  $K(t)$  can be fitted by

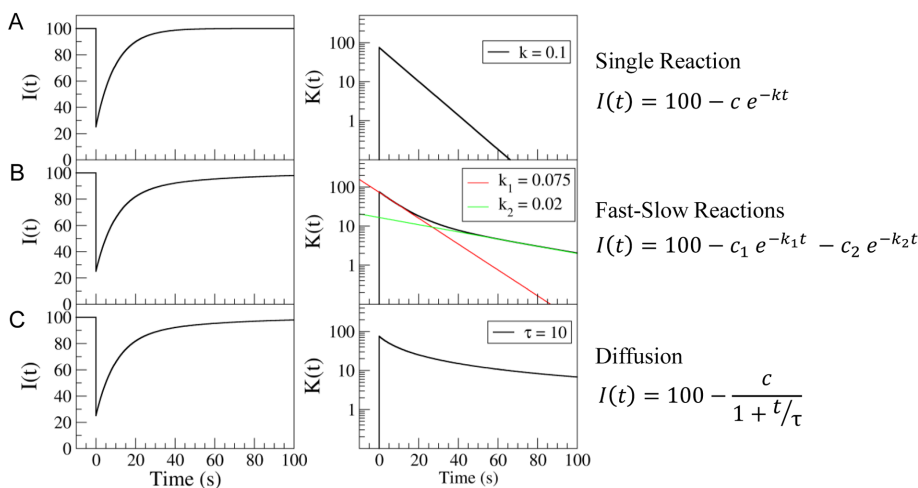


**FIGURE 2:** Theoretical plots of reaction-diffusion kinetic during FRAP.  $I(t)$  shows the normalized FRAP data on a conventional plot (left), while  $K(t)$  is  $100 - I(t)$  and is plotted on a semi-log plot (right). Case A demonstrates a system limited by one reaction rate, case B demonstrates two reaction rates, and case C represents a diffusion-limited system. The two reactions in case B, with reaction constants 0.075 and 0.02, are shown in red and green lines, respectively, to demonstrate how two exponentials sum on the semi-log plot.

$$K(t) = \frac{K_0}{1 + \frac{t}{\tau}} \quad (4)$$

where  $\tau$  is a time constant that depends on the diffusion coefficient for the specific molecule. Taking the logarithm of Eq. 4 will generate a nonlinear curve (Figure 2C). However, it is important to note that a nonlinear function in the semi-log plot does not guarantee that the molecular dynamics are limited by diffusion; it merely indicates that the molecular dynamics are not limited by a reaction. Conceptually, the membrane dynamics of a protein can be limited by slow diffusion in the cytosol, because a bleached protein dissociating from the membrane diffuses away slowly and is slowly replaced by a fluorescent molecule. Quickly diffusing proteins are more readily replaced near the membrane, leading to a rapid association of a fluorescent protein with the membrane. Herein,

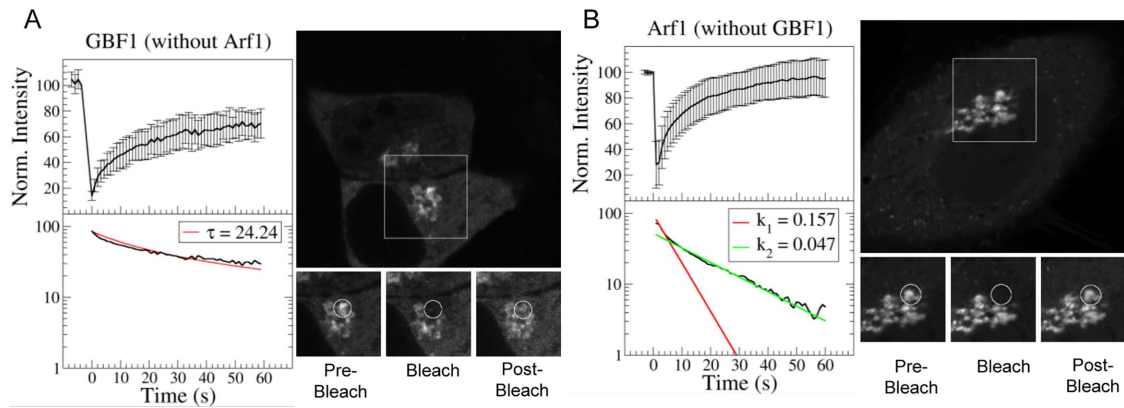


**FIGURE 3:** FRAP dynamics of GBF1 and Arf1 when expressed alone. HeLa cells expressing GFP-tagged wild-type GBF1 (A) or mCherry-tagged Arf1 (B) alone were processed using FRAP. The top plot in each panel shows the mean ( $n = 10$ ), normalized FRAP with error bars representing the SD. The bottom plot in each panel shows the inverted mean FRAP data plotted on a semi-log plot. In panel A, the red line is the fit to the experimental data in black. The best fit was the diffusion model with a time constant of 24.24. In panel B, the red and green lines show the two reactions (rate constants of 0.157 and 0.047, respectively) in the fit to the experimental data. Representative prebleach, bleach, and postbleach (after 54.6 s) images of the FRAP data are also displayed. The top image is the zoomed-out perspective of a representative cell, with the white box showing the region used to display the prebleach, bleach, and postbleach images. The circles in the bottom three images demonstrate the region that was bleached and measured during FRAP.

we used qualitative analyses of FRAP to understand the limiting processes of Arf1 and GBF1 diffusion and association with the Golgi membrane.

#### Kinetic behavior of GBF1 is diffusion-limited

The FRAP behavior of wild-type GBF1 when expressed alone in cells is shown in Figure 3A and is consistent with previously published values. As shown in Table 1, the  $t_{1/2}$  of 7.5 s in this study is similar to the  $t_{1/2}$  of 9.4 s reported previously in Bhatt *et al.* (2016) but lower than the previously reported values of  $t_{1/2}$  of 17 s (Szul *et al.*, 2005) and 30 s (Niu *et al.*, 2005). It is likely that the faster FRAP of the more recent studies is due to faster acquisition rates of now available imaging systems. Plotting the FRAP data on a semi-log produced a

curve, suggesting that GBF1 recovery under these conditions might be diffusion limited.

The qualitative dynamics of GBF1 do not change when GBF1 is coexpressed with its Arf1 substrate, and plotting these FRAP data on a semi-log also produced a curve (Figure 4A and Table 1), suggesting that under these conditions, GBF1 recovery is also diffusion limited. These results imply that GBF1 dynamics on the membrane are predominantly defined by its diffusion rate and indicate that the diffusion parameter is slower than any associations/reactions that GBF1 might have with the Arf1 substrate on the membrane. To test this hypothesis, we postulated and tested two key predictions.

First, because the dynamics of wild-type GBF1 appear not to be defined by its association/reaction with Arf1, the dynamics of a

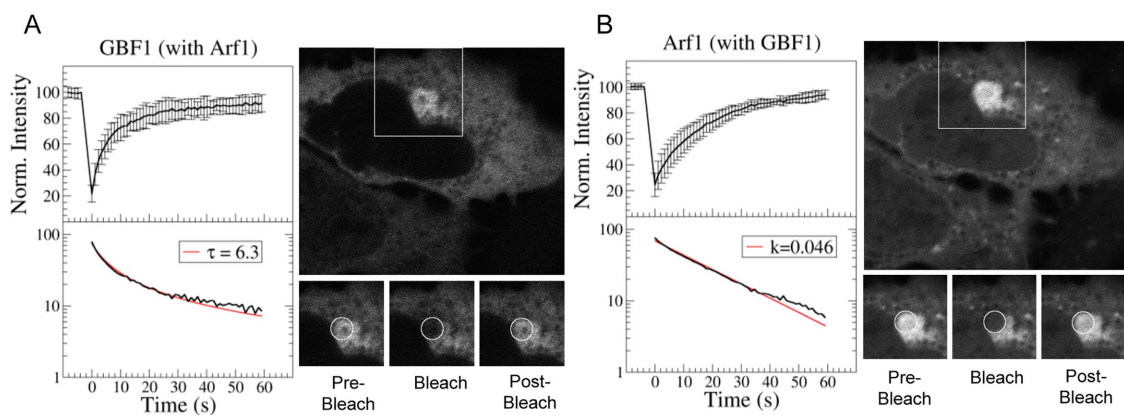


**FIGURE 4:** FRAP dynamics of GBF1 and Arf1 when coexpressed. HeLa cells coexpressing GFP-GBF1 and Arf1-mCherry were simultaneously imaged by FRAP. The top plot in each panel shows the mean ( $n = 11$ ), normalized recovery with error bars representing the SD. The bottom plot shows the inverted mean FRAP data plotted on a semi-log plot. In panel A, the red line is the fit to the experimental data in black. The best fit was the diffusion model with a time constant of 6.3. In panel B, the red line shows the reaction-limiting (reaction constant of 0.046) fit to the experimental data in black. Representative prebleach, bleach, and postbleach (after 59.1 s) images of the FRAP data are also displayed. The top image is the zoomed-out perspective of a representative cell, with the white box showing the region used to display the prebleach, bleach, and postbleach images. The circles in the bottom three images demonstrate the region that was bleached and measured during FRAP.

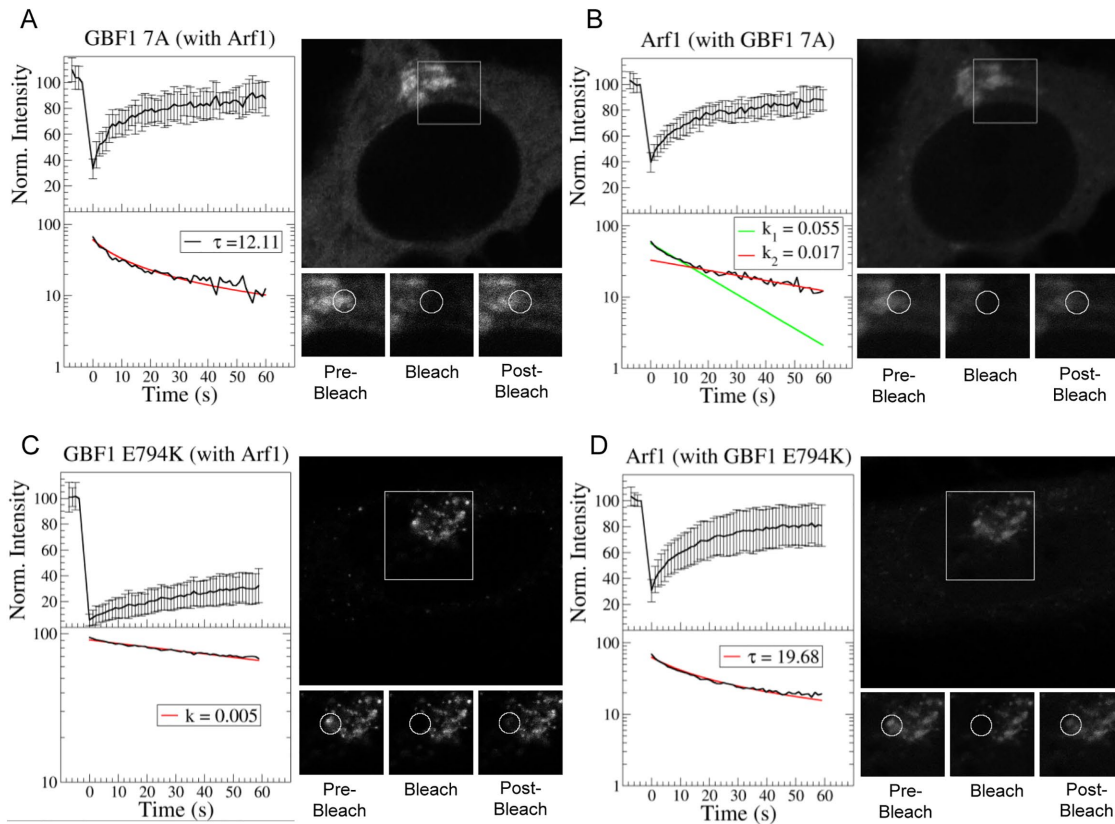


**FIGURE 5:** FRAP dynamics of GBF1 mutants and Arf1 when coexpressed. HeLa cells coexpressing GFP-GBF1/7A and Arf1-mCherry (A, B) or coexpressing GFP-GBF1/E794K and Arf1-mCherry were simultaneously processed using FRAP. The top plot in each panel shows the mean ( $n = 12$ ), normalized recovery with error bars representing SD. The bottom plot in each panel shows the inverted mean FRAP data plotted on a semi-log plot. In panel A, the red line is the diffusion-limited (time constant of 12.11) fit to the experimental data in black. In panel B, the red and green lines show the two reactions (rate constants of 0.055 and 0.017, respectively) in the fit to the experimental data. In panel C, the red line is the best fit reaction (reaction constant of 0.005) to the experimental data in black. In panel D, the red line shows the diffusion (time constant of 19.68)-limiting fit to the experimental data in black. Representative prebleach, bleach, and postbleach (after 58.0 s) images of the FRAP data are also displayed. The top image in each panel is the zoomed-out perspective of a representative cell, with the white box showing the region used to display the prebleach, bleach, and postbleach images. The circles in the bottom three images in each panel demonstrate the region that was bleached and measured during FRAP. The Golgi does not appear to be disrupted in these images due to the very low expression of GBF1/7A and GBF1/E794K. High expression of either construct causes Golgi disruption.

GBF1 mutant unable to bind Arf1 should parallel those of wild-type GBF1. We previously generated and characterized the GBF1/7A mutant unable to bind the Arf1 substrate (Lowery *et al.*, 2011). This mutant is unable to interact with the coexpressed Arf1, and its dynamics should be analogous to the dynamics of wild-type GBF1 expressed in cells without Arf1. Indeed, as shown in Figure 5A and Table 1, the  $t_{1/2}$  of 5.2 of GBF1/7A when coexpressed with Arf1 is similar to the  $t_{1/2}$  of 7.5 s of wild-type GBF1 expressed alone. Plotting the FRAP of GBF1/7A on a semi-log results in a curve, suggesting that GBF1/7A behavior also is diffusion limited.

The time constant for GBF1/7A when coexpressed with Arf1 (12.1 in Figure 5A) is almost twofold higher than the time constant for wild-type GBF1 when coexpressed with Arf1 (6.3 in Figure 4A). We consider it unlikely that the apparent slower movement of the mutant GBF1/7A is due to differences in their cytosolic diffusion, as both proteins migrate at the same position when analyzed on Blue Native gels. We consider it more likely that GBF1/7A is delayed in dissociating from the membrane relative to the wild-type GBF1. A possible explanation for this difference is that activated Arf1 produced by wild-type GBF1, but not by GBF1/7A, creates a mem-

brane environment permissive for GBF1 dissociation. The precise molecular mechanism of GBF1 displacement from the membrane and release into the cytosol remains to be defined.

Second, if the observed diffusion-limited FRAP behavior of wild-type GBF1 coexpressed with Arf reflects a slow diffusion parameter and a fast association/reaction with the Arf substrate (fast enough to be “invisible” within the FRAP dynamics), then the FRAP dynamics of the GBF1/E794K mutant would be expected to be more strongly influenced by the association/reaction component of the dynamics. GBF1/E794K contains a charge reversal from the acidic “glutamic finger” to a positively charged lysine in its Sec7 domain and has been shown to bind Arf1 but does not catalyze GDP expulsion from the bound Arf1. GBF1/E794K has been shown to be stabilized on membranes relative to wild-type GBF1 (Niu *et al.*, 2005; Szul *et al.*, 2005).

We examined the FRAP of GBF1/E794K coexpressed with Arf1 and show that it is significantly slower relative to wild-type GBF1 coexpressed with Arf1 ( $t_{1/2}$  of 19.7 s vs.  $t_{1/2}$  of 4.5) (Figure 5C and Table 1). When plotted on a semi-log scale, the membrane exchange dynamics of GBF1/E794K coexpressed with Arf1 are limited

by one slow reaction. This suggests that the membrane dynamics of GBF1/E794K are no longer regulated by diffusion but instead are defined by membrane events. Previous reports suggested that the stabilization of GBF1/E794K on membranes reflects it remaining in a complex with the endogenous Arf1, with the implication that the expulsion of the GDP is the rate-limiting step in GBF1 on-off membrane dynamics. However, these results are also consistent with the possibility that GBF1/E794K is stabilized on the membrane in a process that is Arf1 independent (see below).

Together, our data are most consistent with a model in which the overall FRAP dynamics of wild-type GBF1 in cells reflect a fast association/reaction of GBF1 with Arf1 on the membrane. While the precise rate of this reaction cannot be resolved, it must be sufficiently fast that the overall reaction rate is limited by the slow diffusion of GBF1 within the cytosol.

### Qualitative dynamics of Arf1 are influenced by GBF1 coexpression

FRAP data for Arf1 when expressed in cells alone are shown in Figure 3B and indicate that Arf1 recovery is limited by a fast reaction for the first few seconds and subsequently by a slow reaction for the rest of the experiment. This suggests that Arf1 diffuses rapidly in the cytosol and its dynamics are predominantly regulated by two distinct membrane events, one extremely rapid and the other with slower kinetics. A plausible model is that when Arf1 is expressed alone, it saturates the available pool of endogenous GBF1, and a proportion of the exogenously expressed Arf1 undergoes rapid unproductive cycles of association and dissociation from the membrane (the “fast” reaction), while the rest interacts with GBF1 on the membrane, is activated, and participates in coating events (the “slow” reaction).

In contrast, when Arf1 is coexpressed with GBF1 (Figure 4B), Arf1 is also reaction limited, but the graph on semi-log indicates only a single reaction rate. This reaction rate appears similar to the “slow” reaction component observed for Arf1 when expressed alone. A plausible model is that when Arf1 and GBF1 are coexpressed, all the exogenously expressed Arf1 can interact with GBF1 productively, and this is reflected in the kinetics, which are now limited by the one, potentially first-order, reaction.

Assuming that the coexpression situation reflects a more physiological relationship between levels of GBF1 and Arf1 in cells, our data suggest a model in which endogenous Arf1 would exhibit analogous dynamics and associate with the Golgi membrane in productive interactions and activation through endogenous GBF1. In this model, there would be an excess of GBF1 on the membrane waiting for Arf1, so that all Arf1 molecules would be able to interact with GBF1 (only one slow reaction would be observed).

This model was tested by coexpressing Arf1 with GBF1/7A, a mutant of GBF1 that does not bind Arf1 (Lowery *et al.*, 2011). A prediction of our model would be that when coexpressed with GBF1/7A, Arf1 dynamics should be analogous to those observed when Arf1 is expressed alone. Indeed, as shown in Figure 5B, two reaction-limited rates were detected, similar to Arf1 dynamics when expressed alone, supporting a model that without productive binding to GBF1/7A, Arf1 exists in a pool that unproductively interacts with the membrane and a pool that binds the endogenous GBF1 on the membrane.

We also examined FRAP of Arf1 when coexpressed with the enzymatically compromised GBF1/E794K mutant (Figure 5D). Based on the current model that GBF1/E794K is stabilized on membranes because it remains in an unproductive complex with Arf1, our expectation was that Arf1 dynamics will be analogous to the dynamics

of GBF1/E794K and be limited by a single slow reaction rate. Surprisingly, plotting the FRAP graph of Arf1 coexpressed with GBF1/E794K on a semi-log indicates a diffusion-limited process and is inconsistent with Arf1 stably interacting with GBF1/E794K on the membrane.

We believe that the diffusion-limited dynamics of Arf1 coexpressed with GBF1/E794K may reflect the varied interactions that the exogenously expressed Arf1 (the species we follow by FRAP) may have with either the exogenously expressed GBF1/E794K or the endogenous wild-type GBF1. The varied interactions would lead to nonlinear reactions, which could cause the semi-log plot to not be fitted with a line and potentially appear diffusion-limited. Therefore, there could be some emergent property of Arf1 in this condition that causes it to be diffusion limited, or Arf1 could be interacting with both species of GBF1 in a highly nonlinear manner. Because Arf1 dynamics do not correlate with the behavior of GBF1/E794K on the membrane, these findings suggest that the reaction-limited GBF1/E794K events on the membrane may occur through a mechanism independent of Arf1 (see below).

### Qualitative dynamics of Arf1/T31N suggest GEF-independent membrane association events

To gain additional insight into the regulatory paradigms of GBF1 and Arf1 membrane dynamics, we assessed the behavior of the Arf1/T31N mutant that contains a single amino acid substitution at the end of the G-1 motif, GX<sub>4</sub>GK(S/T) (Nuoffer and Balch, 1994). Work with the T27N mutant of Arf6 (analogous to the Arf1/T31N mutant) has shown that T27 makes direct contact with the bound GXP, and when mutated causes the loss of affinity for both GDP and GTP (Macia *et al.*, 2004). However, *in vitro*, the Arf6/T27N mutant can be recovered with GDP, but cannot be loaded with GTP, suggesting that in cells it may exist either as a GDP-bound form or as an apo-GTPase. Arf6/T27N is capable of binding its GEF EFA6 in cells (albeit the efficiency of such binding was not determined; Macia *et al.*, 2004), and the dominant negative effects of Arf6/T27N in cells have been ascribed to Arf6/T27N interacting with the endogenous EFA6 and preventing the activation of endogenous Arf6. However, it also remains possible that Arf6/T27N causes dominant negative effects not by saturating the endogenous GEF but by preventing membrane association of the endogenous Arf6 and thereby preventing its activation.

Expression of Arf1/T31N in cells causes the dissociation of the COPI coat and the disruption of the Golgi architecture, presumably due to lack of activation of endogenous Arf1 (Nuoffer and Balch, 1994; Peters *et al.*, 1995). As for Arf6/T27N, it has been postulated that Arf1/T31N causes its dominant negative effects by saturating the endogenous GBF1 and competing with the endogenous Arf1 for binding and activation.

To test this model, we compared the FRAP dynamics of GBF1 when coexpressed with wild-type Arf1 to those when GBF1 is coexpressed with Arf1/T31N. As shown in Figure 6A and Table 1, the FRAP of GBF1 is slightly slower in cells expressing Arf1/T31N ( $t_{1/2}$  of 6.7 s as compared with  $t_{1/2}$  of 4.5 when coexpressed with wild-type Arf1). A previous report described a significantly larger stabilization of GBF1 (an increase from a  $t_{1/2}$  of 17 s to a  $t_{1/2}$  of 45.6 s), but in that study the coexpression of the green fluorescent protein (GFP)-tagged GBF1 and Arf1/T31N was assumed based on the morphology of the Golgi but not actually visualized (Szul *et al.*, 2005). Additionally, choosing cells sufficiently bright to image for FRAP is a subjective process, which may vary between experimentalists. This variance might reflect differences in protein density at the Golgi, which this report shows is a key parameter regulating FRAP data and

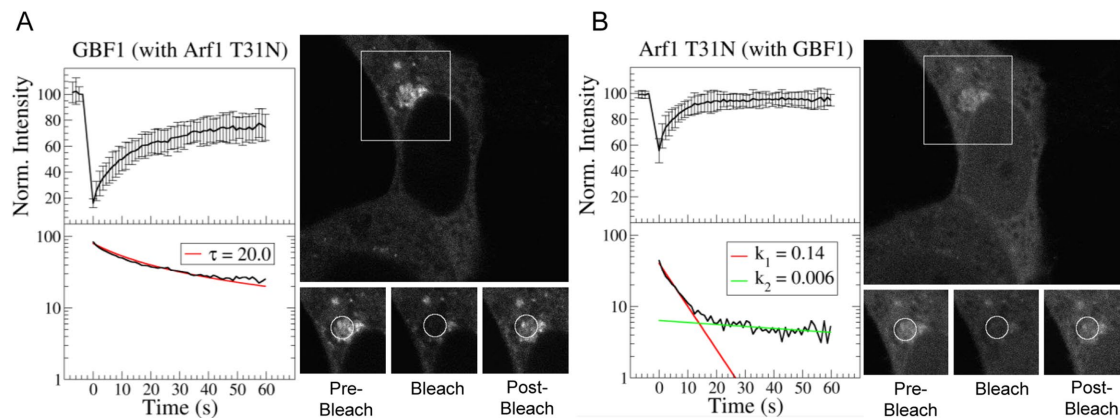


**FIGURE 6:** FRAP dynamics of GBF1 coexpressed with Arf1/T31N mutant. HeLa cells coexpressing GFP-GBF1 and Arf1/T31N-mCherry were simultaneously processed using FRAP. The top plot of each panel shows the mean ( $n = 11$ ), normalized recovery with error bars representing SD. The bottom plot in each panel shows the inverted mean FRAP data plotted on a semi-log plot. In panel A, the red line is the best-fit diffusion (time constant of 20) to the experimental data in black. In panel B, the red and green lines show the two reactions (rate constants of 0.14 and 0.006, respectively) in the fit to the experimental data. Representative prebleach, bleach, and postbleach (after 59.7 s) images of the FRAP data are also displayed. The top image is the zoomed-out perspective of a representative cell, with the white box showing the region used to display the prebleach, bleach, and postbleach images. The circles in the bottom three images demonstrate the region that was bleached and measured during FRAP.

may further lead to discrepancies in the recorded  $t_{1/2}$  values. As far as we are aware, ours represents the first dual FRAP that measures the dynamics of both GBF1 and Arf1/T31N in the same cell. To provide insight into the impact of Arf1/T31N on GBF1, we plotted the GBF1 FRAP data on a semi-log scale, obtaining a curve (Figure 6A). These results indicate a diffusion-limited behavior for GBF1 unlikely to be strongly regulated through reactions with Arf1/T31N on the membrane.

This explanation was supported when we compared the FRAP dynamics of Arf1/T31N coexpressed with GBF1 with those of wild-type Arf1 coexpressed with GBF1. As shown in Figure 6B, a curve was obtained when FRAP data were plotted on a semi-log scale, suggesting that Arf1/T31N dynamics on the membrane are not limited by a reaction with GBF1. Thus, Arf1/T31 association/interaction with GBF1 on the membrane are so rapid as to be invisible within the cycling dynamics of Arf1/T31N.

Our findings are most consistent with a model in which Arf1/T31N causes its dominant negative effects in cells not by interacting with GBF1 and preventing GBF1 from activating endogenous GBF1 but rather from Arf1/T31N saturating membrane-binding sites for endogenous Arf1. This model is supported by the observed intracellular localization of Arf1/T32N expressed in cells: Arf1/T31N can be detected in punctate structures where it colocalizes with GBF1, but the majority of Arf1/T31N appears to be diffusely distributed and not colocalize with GBF1 (Szul *et al.*, 2005). Our model also is consistent with previous reports that Arf1 can associate with membranes before being activated by a GEF (Zhao *et al.*, 2006).

### Simulation of GBF1 and Arf1 dynamics on Golgi membrane

To simulate the diffusion and reactions of GBF1 and Arf1, a simulation code based on a kinetic Monte Carlo algorithm of discrete space, continuous time random walk was developed. The code is written in Fortran 95. We consider three molecular species, GBF1, Arf1-GDP, and Arf1-GTP, that are mobile. Their movements are simulated as jump processes with a fixed distance corresponding to the size of a typical protein. Erickson (2009) provide several proteins of known mass (ranging from 40 to 390 kDa) and dimensions as a reference, and these numbers were used to roughly estimate the dimen-

sions of a standard protein as  $4 \text{ nm} \times 4 \text{ nm} \times 10 \text{ nm}$ . The Arf1 diffusion constant has been calculated to be  $D = 15 \mu\text{m}^2/\text{s}$  (Elsner *et al.*, 2003), which is the number used in the simulation. The jumps are considered as Poisson processes with a given mean transition time. The event-driven algorithm based on a binary tree calendar is adopted for event scheduling to increase computational efficiency (Rapaport, 1995).

In total, there are 15 parameters for chemical dynamics, such as cytosol diffusion constant and membrane association/dissociation rates of Arf1-GTP (all are listed in Table 2). The only parameter empirically obtained is the Arf1 diffusion constant in the cytosol (Elsner *et al.*, 2003), and the other parameter values must be determined by fitting the simulation data to the experimental FRAP data. We analyzed 10–20 different parameter sets at a time, and initial guesses for the new sets of parameters were manually generated. Guesses were then refined by taking the new best fit and further guessing a new set of parameters until there was a good qualitative agreement between the simulation and experiment. Every parameter not experimentally determined was fitted independently for each experiment, unless indicated otherwise in the footnote of Table 2. However, some parameters, such as the estimated diffusion constant for GBF1, were kept the same for each simulation. Analysis of parameters was repeated until a reasonable fit was obtained with FRAP of coexpressed wild-type GBF1 and Arf1 (Figure 7A).

To test the simulations, we investigated how the parameter set changes to fit the FRAP data of GBF1 and the Arf1 when distinct subprocesses are perturbed by the expression of the Arf1/T31N, GBF1/7A, or the GBF1/E794K mutant. An accurate fit is obtained for both proteins when GBF1 is coexpressed with Arf1/T31N (Figure 7B). Similarly, a good fit is evident for the GBF1/7A mutant coexpressed with wild-type Arf1, with only minimal disagreement with Arf1 FRAP at later recovery points (Figure 7C). In contrast, when GBF1/E794K was coexpressed with Arf1, the GBF1/E794K curve fits well to the experimental FRAP, but we could not obtain a good fit for Arf1 (Figure 7D). In our simulations, the theoretical Arf1 FRAP curve is much slower than the experimentally determined FRAP.

We can postulate a possible explanation for the faster than expected FRAP of Arf1 coexpressed with GBF1/E794K. In our

GBF1 species	WT	7A	E794K	WT
Arf1 species	WT	WT	WT	T31N
GBF1 total molecules	11,239 <sup>†</sup>	9553 <sup>†</sup>	11,239 <sup>†</sup>	4355 <sup>†</sup>
GBF1 diffusion constant ( $\mu\text{m}^2/\text{s}$ )	1.56	1.56	1.56	1.56
GBF1 $k_{\text{on}}$ ( $\mu\text{m}/\text{s}$ )	1.25	0.65 <sup>†</sup>	3.73 <sup>†</sup>	1.25
GBF1 $k_{\text{off}}$ (1/s)	1.58	1.58	0.43 <sup>†</sup>	1.58
Arf1 GDP total molecules	7031	7031	7031	12,455
Arf1 GDP* diffusion constant ( $\mu\text{m}^2/\text{s}$ )	15 <sup>*</sup>	15 <sup>*</sup>	15 <sup>*</sup>	15 <sup>*</sup>
Arf1 GDP $k_{\text{on}}$ ( $\mu\text{m}/\text{s}$ )	12	12	12	12
Arf1 GDP $k_{\text{off}}$ (1/s)	0.18	0.18	0.18	0.39 <sup>†</sup>
Arf1 GTP total molecules	7296	7296	7296	12,926
Arf1 GTP* diffusion constant ( $\mu\text{m}^2/\text{s}$ )	15 <sup>*</sup>	15 <sup>*</sup>	15 <sup>*</sup>	15 <sup>*</sup>
Arf1 GTP $k_{\text{on}}$ ( $\mu\text{m}/\text{s}$ )	187.5	187.5	187.5	187.5
Arf1 GTP $k_{\text{off}}$ (1/s)	0.05	0.05	0.05	0.05
GBF1/Arf1 association rate	0.22	0.22	0.22	0.072
GBF1/Arf1 dissociation rate	0.06	0.06	0.005 <sup>†</sup>	0.03 <sup>†</sup>
Arf1 hydrolysis rate	1.25	1.25	1.25	1.25

Parameters used in the Monte Carlo simulation to generate the fit to the experimental data. The \* denotes data gathered from the published literature (Elsner *et al.*, 2003). The  $k_{\text{on}}$  and  $k_{\text{off}}$  values for Arf1-GTP are not necessarily indicative of the real membrane association and dissociation rates. These values were chosen to ensure that Arf1-GTP molecules remained on the membrane. The parameters that were allowed to vary from the wild-type simulation when trying to fit the mutant data are noted with the superscript <sup>†</sup>. The total number of molecules for GBF1, Arf1-GDP, and Arf1-GTP were allowed to vary for all mutant fits.

**TABLE 2:** Simulation parameters for each analyzed species.

experiments, the exogenously expressed GBF1 and Arf1 species are present in cells at approximately twice the level of the endogenous protein (unpublished data). Thus, when GBF1/E794K and Arf1 are coexpressed, distinct interactions between the exogenously

expressed and the endogenous proteins can occur. This variability is not problematic when assessing the FRAP of GBF1/E794K in cells coexpressing Arf1, because all GBF1/E794K molecules will interact exclusively with wild-type Arf1 (either exogenously expressed or

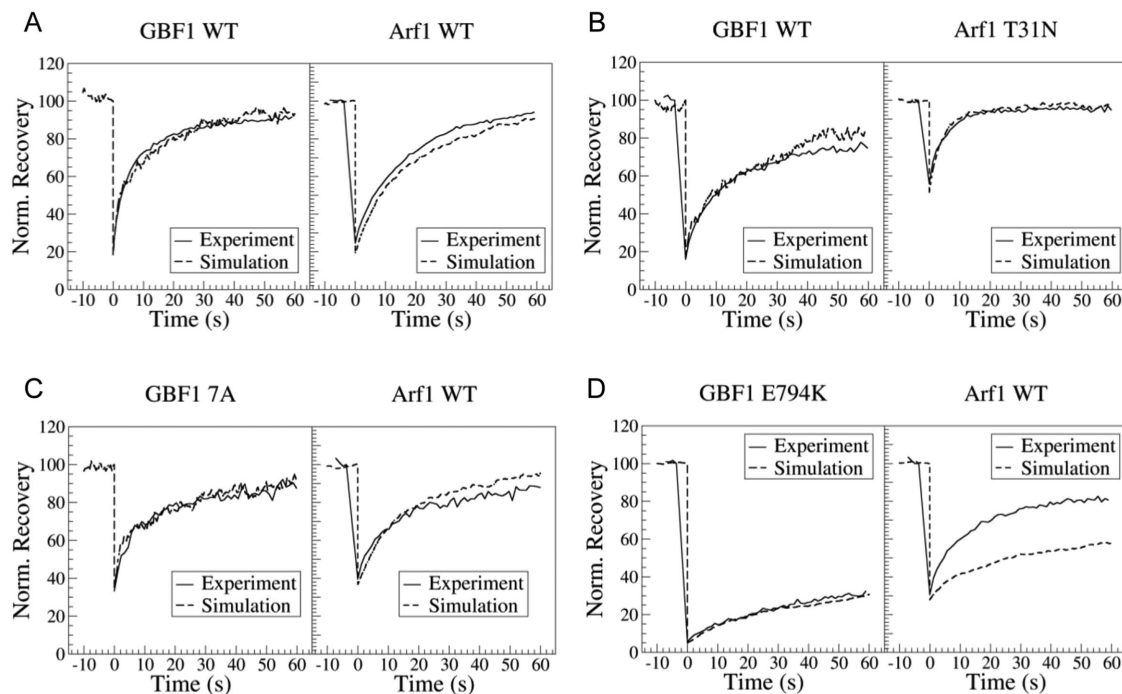


**FIGURE 7:** Simulation fits of FRAP data. HeLa cells coexpressing GFP-GBF1 and Arf1-mCherry (A), GFP-GBF1 and Arf1/T31N-mCherry (B), GFP-GBF1/7A and Arf1-mCherry (C), or GFP-GBF1/E794K GFP and Arf1-mCherry (D) were imaged simultaneously using FRAP as described in Figures 4–6. In each panel, the solid line represents the experimental FRAP data, while the dotted line represents the best fit obtained by the simulation.

endogenous). However, the situation changes when assessing Arf1 behavior in cells coexpressing GBF1/E794K, because the exogenous Arf1 (the species we follow by FRAP) can interact with two distinct species of GBF1, the exogenous GBF1/E794K mutant and the endogenous wild-type GBF1. Our simulation does not account for the presence and the contributions of the endogenous GBF1, and thus the theoretical FRAP of Arf1 shown in Figure 7D simulates Arf1 behavior in a cell depleted of endogenous GBF1 and expressing only the exogenous GBF1/E794K.

## DISCUSSION

Membrane traffic between the compartments of the early secretory pathway is mediated by anterograde vesicles coated with COPII components that transport cargo proteins from the site of their synthesis in the ER to the Golgi and by retrograde vesicles coated with the COPI coat that return membrane and cycling components from the Golgi to the ER (reviewed in Szul and Sztul, 2011). The formation of COPI vesicles is initiated by the GBF1-mediated activation of Arf1 GTPase, which in its GTP-bound form recruits the heptameric coatomer to the membranes to initiate the assembly of the COPI coat. Importantly, both GBF1 and Arf1 are soluble proteins that associate peripherally with Golgi membranes and rapidly cycle between two pools—a larger cytosolic pool and a much smaller membrane-associated pool (Godi *et al.*, 2004; Zhao *et al.*, 2006). We are interested in understanding the parameters that regulate GBF1 and Arf1 membrane dynamics as means to gain insight into their association, interactions, and functions in vesicle formation.

FRAP analyses have provided important insight into the dynamic exchange of peripheral membrane proteins that cycle between cytosolic and membrane-associated pools, and we have used FRAP in conjunction with simulations to probe the relationships between GBF1 and Arf1 at the Golgi of live cells. FRAP is routinely used to compare the  $t_{1/2}$  of recovery of a particular protein when challenged with different conditions to generate models of its behavior and function. Here, we also used FRAP data to compare  $t_{1/2}$  times when distinct subprocesses of COPI coating were disrupted, but in addition we plotted the inverse of the FRAP measurements on a semi-log plot to extract more information about the behaviors of Arf1 and GBF1 under different cellular conditions. The semi-log plots inform on the type of behavior of a protein, as a reaction-limited FRAP is reduced to a straight line with a slope equivalent to the reaction rate, while pure and effective diffusion-limited FRAP is nonlinear on the semi-log plot.

This report presents a quantitative analysis of the behaviors of wild-type and mutant forms of GBF1 and Arf1 obtained from FRAP experiments on the Golgi in live cells under different conditions. Previous FRAP data have been used to propose certain behaviors and interactions between GBF1 and Arf1, but our analyses suggest that some of these models should be revisited.

### Implications for intracellular GBF1 dynamics

Previous FRAP studies of GBF1 expressed alone in cells reported a  $t_{1/2}$  of 30 s (Niu *et al.*, 2005) or 17 s (Szul *et al.*, 2005), and more recently 9.4 s (Bhatt *et al.*, 2016). In this study, we obtained a  $t_{1/2}$  value of 7.5 s, and it is likely that the decrease in the  $t_{1/2}$  represents technological advances in photobleaching and the speed of image acquisition. FRAP of GBF1 expressed alone was nonlinear when plotted on a semi-log plot, suggesting that the process is diffusion-limited. This is consistent with the large size of the GBF1 dimer (~880 kDa), as large proteins or proteins that exist in complexes are likely to experience steric hindrance during diffusion through the crowded cytoplasmic space packed with organelles and cytoskeletal elements

(Saxton, 1993). The expression for the square distance,  $x$ , a molecule with diffusion coefficient,  $D$ , is expected to travel after some time,  $t$ , is

$$\langle x^2 \rangle = 2nDt \quad (5)$$

where  $n$  is the dimension of the brownian motion ( $n$  is 2 on the membrane, while  $n$  is 3 in the cytosol) (Michalet, 2010). The interpretation is that  $n$  describes the environment the molecule is navigating, and the time,  $t$ , is the typical time needed for a molecule with diffusion constant,  $D$ , to travel a distance of  $x^2$ . Because  $D$  and  $x^2$  are directly proportional in Eq. 5, as  $D$  decreases, the distance the molecule is expected to travel in time must decrease. If this decrease is sufficiently large, the molecule's dynamics will be limited by its small diffusion constant.

Such limited diffusion has been reported for the coatomer, a large complex of seven subunits whose measured diffusion coefficient was an order of magnitude slower than the predicted value calculated from the cross-sectional area of the coatomer (Elsner *et al.*, 2003). The previously measured diffusion constant of the coatomer, using FRAP, is  $1.7 \mu\text{m}^2/\text{s}$  (Elsner *et al.*, 2003), which is strikingly similar to the diffusion constant determined for GBF1 by our simulation,  $1.56 \mu\text{m}^2/\text{s}$ . These values are consistent with the similar native sizes of the coatomer (650–700 kDa determined by filtration; Waters *et al.*, 1991) and of GBF1 (~880 kDa determined by Blue Native gels; Bhatt *et al.*, 2016).

To assess how interactions with Arf1 may affect GBF1 dynamics on the membrane, we examined FRAP of GBF1 when coexpressed with Arf1. A slightly quicker (but not significantly different: Supplemental Table 2)  $t_{1/2}$  of 4.5 s was observed for GBF1 coexpressed with Arf1. We interpret the quicker cycling of GBF1 when coexpressed with Arf1 as suggestive that when expressed alone, the majority of GBF1 associates with membranes independently of Arf1 and remains associated for ~7.5 s while “looking” for Arf1, but when GBF1 is coexpressed with Arf1, GBF1 associates with membranes, rapidly finds membrane-associated Arf1, catalyzes GDP/GTP exchange on Arf1 and dissociates from the membrane. FRAP of GBF1 expressed singly or coexpressed with Arf1 is diffusion-limited, indicating that the processes of GBF1 binding and catalyzing Arf1 activation are significantly faster than GBF1 diffusion and thus are not invisible on the semi-log plot.

Although the dynamics of GBF1 are not strongly influenced by Arf1 coexpression, it remains possible that other Arfs may have a stronger effect on GBF1 behavior. GBF1 is known to interact with Arf3, 4, and 5 when probed by bimolecular fluorescence complementation assay (Niu *et al.*, 2005) and has been shown to activate those Arfs at the Golgi (Bhatt *et al.*, 2019). In the future, examining GBF1 behavior when coexpressed with other class I and class II Arfs will allow more detailed analyses of its dynamics and behaviors.

Our coexpression FRAP studies suggest that both GBF1 and Arf1 associate with Golgi membranes independently of each other, presumably by binding organelle-specific components. For GBF1, those could be proteins such as the Rab1 GTPase (Garcia *et al.*, 2011) and the C10orf76 protein (Chan *et al.*, 2019) or a specific phosphatidylinositol-phosphate (PI3P, PI4P, and PI(4,5)P<sub>2</sub>) lipid components (Meissner *et al.*, 2018). For Arf1, it could be the membrane SNARE (Honda *et al.*, 2005) or hydrophobic interactions between the N-terminal  $\alpha$ -helix and the membrane (Mouratou *et al.*, 2005).

The dynamics of the GBF1/7A mutant unable to bind Arf1 coexpressed with Arf1 parallel those of wild-type GBF1 expressed alone ( $t_{1/2}$  of 5.2 s vs.  $t_{1/2}$  of 7.5 s for wild-type GBF1), and in both cases,

the GBF1 species is diffusion-limited. Previous work documented that the GBF1/7A mutant causes the dissociation of the COPI coat (a reflection of inhibition of Arf1 activation) and Golgi disruption (Lowery *et al.*, 2011). Our FRAP analyses support a model in which GBF1/7A causes Golgi disassembly by competing for membrane-binding sites with the endogenous GBF1 and thereby preventing the activation of endogenous Arf1 by the endogenous GBF1.

Previous reports show significantly decreased membrane FRAP rates for the enzymatically dead GBF1/E794K mutant when expressed alone (Szul *et al.*, 2005). The expression of this mutant in cells causes the dissociation of COPI from the membrane and Golgi disruption (Garcia-Mata *et al.*, 2003). The dominant negative effect of GBF1/E794K expression has been interpreted as GBF1/E794K being stabilized on the membrane by binding to and remaining within an unproductive complex with the endogenous Arf1, thereby sequestering Arf1 from the endogenous GBF1 and preventing Arf1 activation. We show that FRAP for GBF1/E794K when coexpressed with Arf1 is significantly slower relative to wild-type GBF1 coexpressed with Arf1 ( $t_{1/2}$  of 19.7 vs. 7.5 s for the wild-type GBF1; Table 1). However, when the inverse of the FRAP was plotted on a semi-log, we obtained a single line, suggesting that GBF1/E794K dynamics are limited by a single, relatively slow reaction. This implies that the major contributors to GBF1/E794K overall dynamics are membrane events instead of diffusion. Such events could be due to GBF1/E794K association/reaction with Arf1 or be Arf1-independent.

To distinguish between these possibilities, we examined the dynamics of Arf1 when coexpressed with GBF1/E794K. If GBF1/E794K remains on the membrane in a complex with Arf1, it would be expected that the dynamics of Arf1 would parallel those of GBF1/E794K. However, neither the  $t_{1/2}$  nor the type of behavior were the same: while the  $t_{1/2}$  of GBF1/E794K recovery was 19.7 s and its behavior was reaction-limited, the  $t_{1/2}$  of Arf1 recovery was 7.2 s and was diffusion-limited. These results are most consistent with GBF1/E794K dynamics on the membrane being regulated through interactions that may not involve direct Arf1 binding. In this model, GBF1/E794K would induce its disruptive phenotype not by sequestering endogenous Arf1 and preventing its activation as currently accepted, but by saturating membrane-binding sites for the endogenous GBF1. This hypothesis is further validated with the simulation data (Table 2). The ratio of the steady state membrane density,  $\sigma$ , to cytosol density,  $\rho$ , is known to be

$$\frac{\sigma}{\rho} = \frac{K_{on}}{K_{off}} \quad (6)$$

by setting the membrane association rate equal to the membrane dissociation rate. In Table 2, we see that  $k_{on}/k_{off}$  increases by slightly more than an order of magnitude for the GBF1/E794K coexpressed with Arf1 ( $k_{on}/k_{off} = 8.67$ ) relative to that of wild-type GBF1 coexpressed with Arf1 ( $k_{on}/k_{off} = 0.79$ ). This suggests that significantly more GBF1/E794K will be bound to the membrane than wild-type endogenous GBF1, possibly saturating membrane-binding sites.

### Implications for Arf1 dynamics on Golgi membranes

Previous FRAP studies reported  $t_{1/2}$  of 15 s (Presley *et al.*, 2002) and 24 s (Szul *et al.*, 2005) for GFP-tagged wild-type Arf1 when expressed alone. Herein, we report a  $t_{1/2}$  of 10.3 s for Arf1-mCherry. Plotting the inverse of the FRAP data on a semi-log generates two lines, indicating that the dynamics of Arf1 expressed alone are limited by an initial, fast reaction and a later, slow reaction. We interpret these data to suggest that overproduction of Arf1 without a corresponding increase in the production of GBF1 results in unproductive

cycles of Arf1 association and dissociation from the membrane (fast reaction), with only a proportion of Arf1 undergoing productive interaction with the endogenous GBF1, being activated and remaining on the membrane as part of the coating process (slow reaction).

In contrast, when Arf1 is coexpressed with GBF1, the  $t_{1/2}$  of its recovery remains similar (10.3 vs. 12.3 s), but its dynamics change and are now limited by a single slow process. These data suggest that when overproduction of Arf1 occurs at the same time as a corresponding increase in the production of GBF1, all membrane-associated Arf1 participates in productive interaction with the endogenous and exogenous GBF1, is activated, and remains on the membrane in the activated state to facilitate coating (hence only a slow reaction is visible). The loss of the fast reaction when ARF1 and GBF1 are coexpressed (perhaps reflecting a more physiological situation) supports a model in which there are more GBF1 on the membrane than Arf1, and thus all Arf1 that associates with the membrane interacts with and is activated by GBF1.

This model is supported by the dynamics of Arf1 when coexpressed with the GBF1/7A mutant incapable of binding or activating Arf1. This mutant is expected to be “invisible” to Arf1, but to compete with the endogenous GBF1 for membrane-binding sites. Thus, Arf1 was expected to behave similarly to when expressed alone, except that a smaller proportion of Arf1 should be activated and remain on the membrane. Indeed, we observed a slight increase in the FRAP dynamics of Arf1 ( $t_{1/2}$  of 7.6 vs. 10.3 s for the wild-type GBF1) and two lines when the inverse of the FRAP was plotted on a semi-log. Thus, Arf1 coexpressed with GBF1/7A undergoes fast, ineffective sampling of the membrane and then a reduced level of productive interactions with the endogenous GBF1.

It is important to note that the Arf1 FRAP curves in Figures 3B and 4B, before being inverted and graphed on a semi-log plot, look relatively similar. While there are some slight qualitative differences, it would have been impossible to discern how many limiting reactions are present by visual inspection or calculating the  $t_{1/2}$ . Therefore, when comparing reaction-limited FRAP data, it can be more insightful to use this type of quantitative approach as opposed to the mere  $t_{1/2}$  value.

The dynamics of GBF1 coexpressed with Arf1/T31N and of Arf1/T31N coexpressed with GBF1 were surprising. Previous studies showed that GBF1 is stabilized in cells when coexpressed with Arf1/T31N (Niu *et al.*, 2005; Szul *et al.*, 2005), and these results were interpreted as GBF1 remaining on the membrane in a complex with the Arf1/T31N mutant. This model implies that GBF1 and Arf1/T31N should show similar FRAP behaviors on the membrane and be reaction-limited. The FRAP dynamics of GBF1 coexpressed with Arf1/T31N ( $t_{1/2}$  of 6.7 s) were different from those of Arf1/T31N ( $t_{1/2}$  of 2.9 s), and the dynamics were diffusion-limited. This suggests that even if GBF1 and Arf1/T31N interact on the membrane, such interactions are so fast as to be “invisible” in the overall dynamics. Alternatively, GBF1 and Arf1/T31N might participate in limited interaction/reaction events on the membrane. The latter interpretation is supported by the limited colocalization of GBF1 and Arf1/T31N in cells (Szul *et al.*, 2005; Chun *et al.*, 2008). These data suggest that Arf1/T31N would induce its disruptive phenotype not by sequestering endogenous GBF1 and preventing the activation of endogenous Arf1 as currently accepted, but by reducing the membrane concentration of endogenous Arf1.

### Role of simulations in analyzing GBF1 and Arf1 dynamics

The simulations quantify how much endogenous proteins can contribute to kinetic data, especially when overexpressing certain types

of mutants, and provide insight into possible mechanisms through which protein behavior is influenced by the coexpressed proteins. Our simulations generally fitted well with our experimental data, with the exception of Arf1 dynamics when coexpressed with the GBF1/E794K mutant. In this case, both the endogenous GBF1 and the GBF1/E794K are present in the cell and Arf1 dynamics can be impacted by both GBF1 species, resulting in dynamics that reflect the composite of those distinct behaviors. Our inability to make the simulation fit the experimental FRAP data indicates a large contribution of the endogenous GBF1 to Arf1 dynamics. Future studies can avoid the contribution of the endogenous proteins when analyzing kinetic data by knocking down the endogenous protein and assuring that only the exogenously produced protein influences the dynamics.

Coating is a compilation of distinct subprocesses linked to each other temporally and causally, and to understand the overall process, we need to know how one component influences the behavior of other components within the coating pathway. Understanding the overall order of the distinct subprocesses and the relative impact of each subprocess on subsequent events will require additional studies to incorporate the dynamics of additional molecules within the coating pathway including ArfGAP1 and coatomer. Ultimately, incorporation of additional Arf1 and GBF1 interactors will provide a network-level understanding of the coating process.

## MATERIALS AND METHODS

Request a protocol through *Bio-protocol*.

### Plasmids

mCherry-tagged wild-type Arf1 and Arf1/T31N constructs were generous gifts from Paul Melançon (University of Alberta, Alberta, Canada). GFP-tagged wild-type GBF1 and GBF1/E794K were previously described (Garcia-Mata *et al.*, 2003). GFP-tagged GBF1/7A was previously described (Lowery *et al.*, 2011).

### Cell culture and transfection

HeLa cells were grown in DMEM (Corning) supplemented with 10% fetal bovine serum and 1% penicillin/streptomycin (Corning) at 37°C in 5% CO<sub>2</sub>. Cells were grown on 25-mm-diameter glass coverslips of thickness #1.5 (Electron Microscopy Sciences) for ~24 h pretransfection until ~70% confluent. Single plasmid DNA (1.0 µg) or 0.5 µg of each plasmid DNA for cotransfection experiments was added to 100 µl of RPMI-1640 with L-glutamine (Corning) and 5 µl of TransIT-LT1 (Mirus), and the transfection was performed as per the manufacturer's directions. Cells were grown for 24 h before FRAP.

### FRAP

The Nikon A1R-HD25 microscope at the University of Alabama at Birmingham High Resolution Imaging Facility Service Center was used for FRAP analysis. The cells were placed inside a silicon-sealed chamber at 37°C and 5% CO<sub>2</sub>. For GFP-tagged constructs, a 488-nm laser beam was used to photobleach an area of 2 µm on the Golgi. For mCherry-tagged constructs, the laser wavelength was set to 561 nm. Frames were captured every 1 s, and the data were averaged over 9–12 cells. For GBF1/E794K coexpressed with Arf1, 12 cells were averaged. For GBF1 coexpressed with Arf, 11 cells were averaged. For GBF1/7A coexpressed with Arf1, nine cells were averaged. For GBF1 coexpressed with Arf1/T31N, 10 cells were averaged. All cells chosen for FRAP had low levels of expression of the exogenous proteins to reduce the effects of the law of mass action as much as possible.

All FRAP data are normalized and corrected for nonspecific photobleaching by subtracting the background intensity from the ex-

perimental and reference ROIs and taking the ratio, respectively. The experimental ROI is the area of the Golgi being bleached, while the reference ROI is in the cytosol, far from the experimental region, to correct for any photobleaching. The photobleached corrected data are collected by dividing the experimental ROI by the reference ROI for each frame. Then, the data are divided by the intensity immediately before bleaching to obtain a normalized recovery plot.

### Monte Carlo simulation

The simulation is written in Fortran 95 and uses a discrete space, continuous-time random walk for all molecular species (Kosztolowicz, 2015). The diffusion is simulated as jump processes with a fixed distance approximately the size of the molecules. The jumps are considered as Poisson processes with a given mean transition time. The event-driven algorithm based on a binary tree calendar is adopted for event scheduling to increase computational efficiency. In total, there are 14 parameters capturing the diffusion, membrane association/dissociation, and reaction rates for all molecular species. Questions regarding code accessibility should be addressed to the corresponding author.

### Plotting FRAP data on semi-log

As with any data analysis workflow, there is always a push–pull relationship between developing a method that is convenient to use and maintaining scientific rigor. The semi-log method for FRAP data is not optimal to assess the behavior of proteins limited by highly nonlinear reactions of second order or higher. Nonlinear differential equations are often impossible to analytically solve, and simple equations (such as Eq. 2 or Eq. 4) will not fit these data. If this occurs, it would be recommended to use other metrics (such as the  $t_{1/2}$  and the immobile phase) to analyze the FRAP data. Considering that cellular processes are usually nonlinear, it may seem that the semi-log method will almost always fail and therefore be useless. However, because the system is in steady state before the photobleaching, the nonlinear reaction-diffusion equations for molecules in the FRAP experiment can sometimes be simplified to linear equations.

Generally, it is assumed that the concentrations of all molecular species in a reaction-diffusion partial differential equation are time dependent. This assumption is invalid for FRAP, because the system was in steady state before bleaching and remains so during the subsequent recovery. To accurately solve the reaction-diffusion equation for the fluorescent Arf1-GDP molecules, the total number of GBF1 molecules in the cell should be treated as a constant (assuming that photobleaching does not dramatically affect the reactivity of GBF1). Hence, any reaction term in the Arf1-GDP reaction-diffusion equation that involves the product of the concentration of Arf1-GDP and GBF1 would become linear, because the concentration of GBF1 is constant in that specific equation (note that the opposite will be true for the reaction-diffusion equation of GBF1). Hence, the semi-log plot will still appear linear for molecules involved in nonlinear reactions when the nonlinearity arises from the product of the concentration of substrates. This simplification also eliminates most, if not all, of the coupling terms between differential equations, which may make the reaction-diffusion ordinary differential equations analytically solvable. Hence, the semi-log method should be helpful for a large set of limiting reactions. In this report, we show that the semi-log method can be used to describe the limiting processes of Arf1 and GBF1 diffusion and association with Golgi membranes.

### ACKNOWLEDGMENTS

We thank Luis Mayorga and Richard Kahn for their important insights and suggestions during the course of this study. This work

was supported by grants from the National Science Foundation (MCB-1615607 to E. S.) and the National Institutes of Health (R01GM122802 to E. S.). The High Resolution Imaging Facility Service Center is an institutional core at the University of Alabama at Birmingham supported by the Office of the Vice President of Research and Development and the following grants: Cancer Center Support Grant P30 CA013148 and Rheumatic Disease Core Center Grant P30 AR048311.

## REFERENCES

- Abruzzi KC, Smith A, Chen W, Solomon F (2002). Protection from free beta-tubulin by the beta-tubulin binding protein Rbl2p. *Mol Cell Biol* 22, 138–147.
- Arakel EC, Schwappach B (2018). Formation of COPI-coated vesicles at a glance. *J Cell Sci* 131, jcs.209890.
- Axelrod D, Koppel DE, Schlessinger J, Elson E, Webb WW (1976). Mobility measurement by analysis of fluorescence photobleaching recovery kinetics. *Biophys J* 16, 1055–1069.
- Barlowe C (2000). Traffic COPs of the early secretory pathway. *Traffic* 1, 371–377.
- Barlowe C (2002). COPII-dependent transport from the endoplasmic reticulum. *Curr Opin Cell Biol* 14, 417–422.
- Beraud-Dufour S, Robineau S, Chardin P, Paris S, Chabre M, Cherfils J, Antony B (1998). A glutamic finger in the guanine nucleotide exchange factor ARNO displaces Mg<sup>2+</sup> and the beta-phosphate to destabilize GDP on ARF1. *EMBO J* 17, 3651–3659.
- Bethune J, Wieland FT (2018). Assembly of COPI and COPII vesicular coat proteins on membranes. *Annu Rev Biophys* 47, 63–83.
- Bhatt JM, Hancock KW, Meissner JM, Kaczmarczyk A, Lee E, Viktorova E, Ramanadham S, Belov GA, Sztula E (2019). Promiscuity of the catalytic Sec7 domain within the guanine nucleotide exchange factor GBF1 in ARF activation, Golgi homeostasis, and effector recruitment. *Mol Biol Cell* 30, 1523–1535.
- Bhatt JM, Viktorova EG, Busby T, Wyrozumska P, Newman LE, Lin H, Lee E, Wright J, Belov GA, Kahn RA, et al. (2016). Oligomerization of the Sec7 domain Arf guanine nucleotide exchange factor GBF1 is dispensable for Golgi localization and function but regulates degradation. *Am J Physiol Cell Physiol* 310, C456–C469.
- Bouvet S, Golinelli-Cohen MP, Contremoulin V, Jackson CL (2013). Targeting of the Arf-GEF GBF1 to lipid droplets and Golgi membranes. *J Cell Sci* 126, 4794–4805.
- Bui QT, Golinelli-Cohen MP, Jackson CL (2009). Large Arf1 guanine nucleotide exchange factors: evolution, domain structure, and roles in membrane trafficking and human disease. *Mol Genet Genomics* 282, 329–350.
- Bussey H, Saville D, Greene D, Tipper DJ, Bostian KA (1983). Secretion of *Saccharomyces cerevisiae* killer toxin: processing of the glycosylated precursor. *Mol Cell Biol* 3, 1362–1370.
- Casanova JE (2007). Regulation of Arf activation: the Sec7 family of guanine nucleotide exchange factors. *Traffic* 8, 1476–1485.
- Chan CJ, Le R, Burns K, Ahmed K, Coyaud E, Laurent EMN, Raught B, Melancon P (2019). BiLD performed on Golgi enriched fractions identify C10orf76 as a GBF1 binding protein essential for Golgi maintenance and secretion. *Mol Cell Proteomics* 18, 2285–2297.
- Cherfils J, Menetrey J, Mathieu M, Le Bras G, Robineau S, Beraud-Dufour S, Antony B, Chardin P (1998). Structure of the Sec7 domain of the Arf exchange factor ARNO. *Nature* 392, 101–105.
- Chun J, Shapovalova Z, Deigaard SY, Presley JF, Melancon P (2008). Characterization of class I and II ADP-ribosylation factors (Arfs) in live cells: GDP-bound class II Arfs associate with the ER-Golgi intermediate compartment independently of GBF1. *Mol Biol Cell* 19, 3488–3500.
- Claude A, Zhao BP, Kuziemyk CE, Dahan S, Berger SJ, Yan JP, Arnold AD, Sullivan EM, Melancon P (1999). GBF1: a novel Golgi-associated BFA-resistant guanine nucleotide exchange factor that displays specificity for ADP-ribosylation factor 5. *J Cell Biol* 146, 71–84.
- Dancourt J, Barlowe C (2010). Protein sorting receptors in the early secretory pathway. *Annu Rev Biochem* 79, 777–802.
- D’Arcangelo JG, Stahmer KR, Miller EA (2013). Vesicle-mediated export from the ER: COPII coat function and regulation. *Biochim Biophys Acta* 1833, 2464–2472.
- Dell’Angelica EC, Bonifacino JS (2019). Coatopathies: genetic disorders of protein coats. *Annu Rev Cell Dev Biol* 35, 131–168.
- Deng Y, Golinelli-Cohen MP, Smirnova E, Jackson CL (2009). A COPI coat subunit interacts directly with an early-Golgi localized Arf exchange factor. *EMBO Rep* 10, 58–64.
- Derby MC, Gleeson PA (2007). New insights into membrane trafficking and protein sorting. *Int Rev Cytol* 261, 47–116.
- D’Souza RS, Casanova JE (2016). The BRAG/IQSec family of Arf GEFs. *Small GTPases* 7, 257–264.
- Edidin M, Zagayansky Y, Lardner TJ (1976). Measurement of membrane protein lateral diffusion in single cells. *Science* 191, 466–468.
- Elsner M, Hashimoto H, Simpson JC, Cassel D, Nilsson T, Weiss M (2003). Spatiotemporal dynamics of the COPI vesicle machinery. *EMBO Rep* 4, 1000–1004.
- Erickson HP (2009). Size and shape of protein molecules at the nanometer level determined by sedimentation, gel filtration, and electron microscopy. *Biol Proced Online* 11, 32–51.
- Faini M, Beck R, Wieland FT, Briggs JA (2013). Vesicle coats: structure, function, and general principles of assembly. *Trends Cell Biol* 23, 279–288.
- Franco M, Chardin P, Chabre M, Paris S (1995). Myristoylation of ADP-ribosylation factor 1 facilitates nucleotide exchange at physiological Mg<sup>2+</sup> levels. *J Biol Chem* 270, 1337–1341.
- Franco M, Chardin P, Chabre M, Paris S (1996). Myristoylation-facilitated binding of the G protein ARF1GDP to membrane phospholipids is required for its activation by a soluble nucleotide exchange factor. *J Biol Chem* 271, 1573–1578.
- Garcia IA, Martinez HE, Alvarez C (2011). Rab1b regulates COPI and COPII dynamics in mammalian cells. *Cell Logist* 1, 159–163.
- Garcia-Mata R, Szul T, Alvarez C, Sztul E (2003). ADP-ribosylation factor/COPI-dependent events at the endoplasmic reticulum-Golgi interface are regulated by the guanine nucleotide exchange factor GBF1. *Mol Biol Cell* 14, 2250–2261.
- Gleeson PA, Lock JG, Luke MR, Stow JL (2004). Domains of the TGN: coats, tethers and G proteins. *Traffic* 5, 315–326.
- Godi A, Di Campli A, Konstantakopoulos A, Di Tullio G, Alessi DR, Kular GS, Daniele T, Marra P, Lucocq JM, De Matteis MA (2004). FAPPs control Golgi-to-cell-surface membrane traffic by binding to ARF and PtdIns(4)P. *Nat Cell Biol* 6, 393–404.
- Goldberg J (1998). Structural basis for activation of ARF GTPase: mechanisms of guanine nucleotide exchange and GTP-myristoyl switching. *Cell* 95, 237–248.
- Honda A, Al-Awar OS, Hay JC, Donaldson JG (2005). Targeting of Arf-1 to the early Golgi by membrin, an ER-Golgi SNARE. *J Cell Biol* 168, 1039–1051.
- Jacobson K, Wu E, Poste G (1976). Measurement of the translational mobility of concanavalin A in glycerol-saline solutions and on the cell surface by fluorescence recovery after photobleaching. *Biochim Biophys Acta* 433, 215–222.
- Kawamoto K, Yoshida Y, Tamaki H, Torii S, Shinotsuka C, Yamashina S, Nakayama K (2002). GBF1, a guanine nucleotide exchange factor for ADP-ribosylation factors, is localized to the cis-Golgi and involved in membrane association of the COPI coat. *Traffic* 3, 483–495.
- Kosztolowicz T (2015). Random walk model of subdiffusion in a system with a thin membrane. *Phys Rev E Stat Nonlin Soft Matter Phys* 91, 022102.
- Kuehn MJ, Schekman R (1997). COPII and secretory cargo capture into transport vesicles. *Curr Opin Cell Biol* 9, 477–483.
- Kuhn T, Ihalainen TO, Hyvaluoma J, Dross N, Willman SF, Langowski J, Vihinen-Ranta M, Timonen J (2011). Protein diffusion in mammalian cell cytoplasm. *PLoS One* 6, e22962.
- Lord C, Ferro-Novick S, Miller EA (2013). The highly conserved COPII coat complex sorts cargo from the endoplasmic reticulum and targets it to the golgi. *Cold Spring Harb Perspect Biol* 5, a013367.
- Lowe M, Kreis TE (1998). Regulation of membrane traffic in animal cells by COPI. *Biochim Biophys Acta* 1404, 53–66.
- Lowery J, Szul T, Seetharaman J, Jian X, Su M, Forouhar F, Xiao R, Acton TB, Montelione GT, Lin H, et al. (2011). Novel C-terminal motif within Sec7 domain of guanine nucleotide exchange factors regulates ADP-ribosylation factor (ARF) binding and activation. *J Biol Chem* 286, 36898–36906.
- Meissner JM, Bhatt JM, Lee E, Styers ML, Ivanova AA, Kahn RA, Sztul E (2018). The ARF guanine nucleotide exchange factor GBF1 is targeted to Golgi membranes through a PIP-binding domain. *J Cell Sci* 131, jcs.210245.
- Macia E, Luton F, Partisani M, Cherfils J, Chardin P, Franco M (2004). The GDP-bound form of Arf6 is located at the plasma membrane. *J Cell Sci* 117, 2389–2398.
- Michalet X (2010). Mean square displacement analysis of single-particle trajectories with localization error: Brownian motion in isotropic medium. *Phys Rev E Stat Nonlin Soft Matter Phys* 82, 041914.
- Miller EA, Barlowe C (2010). Regulation of coat assembly—sorting things out at the ER. *Curr Opin Cell Biol* 22, 447–453.

- Moriya H (2015). Quantitative nature of overexpression experiments. *Mol Biol Cell* 26, 3932–3939.
- Mouratou B, Biou V, Joubert A, Cohen J, Shields DJ, Geldner N, Jurgens G, Melancon P, Cherfils J (2005). The domain architecture of large guanine nucleotide exchange factors for the small GTP-binding protein Arf. *BMC Genomics* 6, 20.
- Nawroth A, Zeghouf M, Cherfils J (2016). Allosteric regulation of Arf GTPases and their GEFs at the membrane interface. *Small GTPases* 7, 283–296.
- Nehls S, Snapp EL, Cole NB, Zaal KJ, Kenworthy AK, Roberts TH, Ellenberg J, Presley JF, Siggia E, Lippincott-Schwartz J (2000). Dynamics and retention of misfolded proteins in native ER membranes. *Nat Cell Biol* 2, 288–295.
- Niu TK, Pfeifer AC, Lippincott-Schwartz J, Jackson CL (2005). Dynamics of GBF1, a Brefeldin A-sensitive Arf1 exchange factor at the Golgi. *Mol Biol Cell* 16, 1213–1222.
- Nuoffer C, Balch WE (1994). GTPases: multifunctional molecular switches regulating vesicular traffic. *Annu Rev Biochem* 63, 949–990.
- Ostermann J, Orci L, Tani K, Amherdt M, Ravazzola M, Elazar Z, Rothman JE (1993). Stepwise assembly of functionally active transport vesicles. *Cell* 75, 1015–1025.
- Peter F, Plutner H, Zhu H, Kreis TE, Balch WE (1993). Beta-COP is essential for transport of protein from the endoplasmic reticulum to the Golgi in vitro. *J Cell Biol* 122, 1155–1167.
- Peters PJ, Hsu VW, Ooi CE, Finazzi D, Teal SB, Oorschot V, Donaldson JG, Klausner RD (1995). Overexpression of wild-type and mutant ARF1 and ARF6: distinct perturbations of nonoverlapping membrane compartments. *J Cell Biol* 128, 1003–1017.
- Peters R, Peters J, Tews KH, Bahr W (1974). A microfluorimetric study of translational diffusion in erythrocyte membranes. *Biochim Biophys Acta* 367, 282–294.
- Poo M, Cone RA (1974). Lateral diffusion of rhodopsin in the photoreceptor membrane. *Nature* 247, 438–441.
- Presley JF, Ward TH, Pfeifer AC, Siggia ED, Phair RD, Lippincott-Schwartz J (2002). Dissection of COPI and Arf1 dynamics in vivo and role in Golgi membrane transport. *Nature* 417, 187–193.
- Rapaport DC (1995). *The Art of Molecular Dynamics Simulation*, Cambridge, UK: Cambridge University Press.
- Renault L, Christova P, Guibert B, Pasqualato S, Cherfils J (2002). Mechanism of domain closure of Sec7 domains and role in BFA sensitivity. *Biochemistry* 41, 3605–3612.
- Rowe T, Aridor M, McCaffery JM, Plutner H, Nuoffer C, Balch WE (1996). COPII vesicles derived from mammalian endoplasmic reticulum microsome recruit COPI. *J Cell Biol* 135, 895–911.
- Saxton MJ (1993). Lateral diffusion in an archipelago. *Single-particle diffusion*. *Biophys J* 64, 1766–1780.
- Scales SJ, Gomez M, Kreis TE (2000). Coat proteins regulating membrane traffic. *Int Rev Cytol* 195, 67–144.
- Scales SJ, Pepperkok R, Kreis TE (1997). Visualization of ER-to-Golgi transport in living cells reveals a sequential mode of action for COPII and COPI. *Cell* 90, 1137–1148.
- Schlessinger J, Koppel DE, Axelrod D, Jacobson K, Webb WW, Elson EL (1976). Lateral transport on cell membranes: mobility of concanavalin A receptors on myoblasts. *Proc Natl Acad Sci USA* 73, 2409–2413.
- Shima DT, Scales SJ, Kreis TE, Pepperkok R (1999). Segregation of COPI-rich and anterograde-cargo-rich domains in endoplasmic-reticulum-to-Golgi transport complexes. *Curr Biol* 9, 821–824.
- Spang A, Matsuoka K, Hamamoto S, Schekman R, Orci L (1998). Coat-omer, Arf1p, and nucleotide are required to bud coat protein complex I-coated vesicles from large synthetic liposomes. *Proc Natl Acad Sci USA* 95, 11199–11204.
- Sprague BL, Pego RL, Stavreva DA, McNally JG (2004). Analysis of binding reactions by fluorescence recovery after photobleaching. *Biophys J* 86, 3473–3495.
- Stagg SM, LaPointe P, Balch WE (2007). Structural design of cage and coat scaffolds that direct membrane traffic. *Curr Opin Struct Biol* 17, 221–228.
- Sztul E, Chen PW, Casanova JE, Cherfils J, Dacks JB, Lambright DG, Lee FS, Randazzo PA, Santy LC, Schurmann A, et al. (2019). ARF GTPases and their GEFs and GAPs: concepts and challenges. *Mol Biol Cell* 30, 1249–1271.
- Sztul E, Garcia-Mata R, Brandon E, Shestopal S, Alvarez C, Sztul E (2005). Dissection of membrane dynamics of the ARF-guanine nucleotide exchange factor GBF1. *Traffic* 6, 374–385.
- Sztul E, Grabski R, Lyons S, Morohashi Y, Shestopal S, Lowe M, Sztul E (2007). Dissecting the role of the ARF guanine nucleotide exchange factor GBF1 in Golgi biogenesis and protein trafficking. *J Cell Sci* 120, 3929–3940.
- Sztul E, Sztul E (2011). COPII and COPI traffic at the ER-Golgi interface. *Physiology (Bethesda)* 26, 348–364.
- Tan JZA, Gleeson PA. (2019). Cargo Sorting at the trans-Golgi Network for Shunting into Specific Transport Routes: Role of Arf Small G Proteins and Adaptor Complexes. *Cells* 8.
- Tang BL, Wang Y, Ong YS, Hong W (2005). COPII and exit from the endoplasmic reticulum. *Biochim Biophys Acta* 1744, 293–303.
- VanWinkle PE, Parish F, Edwards YJK, Sztul E. (2020). JAGN1, tetraspanins and Erv proteins: is common topology indicative of common function in cargo sorting? *Am J Physiol Cell Physiol* 319, C667–C674.
- Wang T, Li L, Hong W (2017). SNARE proteins in membrane trafficking. *Traffic* 18, 767–775.
- Waters MG, Serafini T, Rothman JE (1991). ‘Coatomer’: a cytosolic protein complex containing subunits of non-clathrin-coated Golgi transport vesicles. *Nature* 349, 248–251.
- Wright J, Kahn RA, Sztul E (2014). Regulating the large Sec7 ARF guanine nucleotide exchange factors: the when, where and how of activation. *Cell Mol Life Sci* 71, 3419–3438.
- Yu X, Breitman M, Goldberg J (2012). A structure-based mechanism for Arf1-dependent recruitment of coatomer to membranes. *Cell* 148, 530–542.
- Zagyansky Y, Edidin M (1976). Lateral diffusion of concanavalin A receptors in the plasma membrane of mouse fibroblasts. *Biochim Biophys Acta* 433, 209–214.
- Zhao X, Claude A, Chun J, Shields DJ, Presley JF, Melancon P (2006). GBF1, a cis-Golgi and VTCs-localized ARF-GEF, is implicated in ER-to-Golgi protein traffic. *J Cell Sci* 119, 3743–3753.

# Supplemental Materials

*Molecular Biology of the Cell*

Sager *et al.*

1: Examined combinations of GBF1 and Arf1 constructs.

GBF1 Protein	Arf1 Protein
GBF1 WT GFP	-
-	Arf1 WT mCherry
GBF1 WT GFP	Arf1 WT mCherry
GBF1 E794K GFP	Arf1 WT mCherry
GBF1 7A GFP	Arf1 WT mCherry
GBF1 WT GFP	Arf1 T31N mCherry

**Supplemental Table 1:** The table lists all the combinations of components analyzed in this study. A “-“ means no exogenous protein of that species was introduced into cells.

Experimental Condition	Mean $\pm$ STD	P-values				
		8.3E-4	9.0E-1	4.1E-4	4.4E-3	
GBF1 WT (without Arf1 coexpression)	8.0 $\pm$ 2.5	8.3E-4	9.0E-1	4.1E-4	4.4E-3	
GBF1 WT (with Arf1 WT coexpression)	4.2 $\pm$ 1.5	**			2.7E-3	4.4E-5
GBF1 WT (with Arf1/T31N coexpression)	7.8 $\pm$ 2.8				**	3.7E-4
GBF1/E794K (with Arf1 WT coexpression)	20.6 $\pm$ 8.9			***		****
GBF1/7A (with Arf1 WT coexpression)	4.9 $\pm$ 1.4				**	*
						6.7E-5
						***
						2.8E-1
						1.2E-2

**Supplemental Table 2:** The table lists the mean  $\pm$  standard deviation (STD)  $t_{1/2}$  values for GFP-GBF1 constructs expressed alone or co-expressed with Arf1-mCherry constructs. P-values are calculated with a two-tailed t-test and using  $\alpha = 0.05$ . To reduce space, scientific notation (i.e.  $3 \times 10^{-5}$ ) is abbreviated with an E (i.e. 3E-5). With five experimental conditions, there are a total of ten p-values calculated. Each pair of comparisons is denoted by similar color. Light green corresponds to the results of the t-test analysis between GBF1 expressed alone and GBF1 co-expressed with Arf1. Light blue corresponds to the results of the t-test analysis between GBF1 expressed alone and GBF1 co-expressed with Arf1/T31N. Light tan corresponds to the results of the t-test analysis between GBF1 expressed alone and GBF1/E794K co-expressed with Arf1. Light gray corresponds to the results of the t-test analysis between GBF1 expressed alone and GBF1/7A co-expressed with Arf1. Light pink corresponds to the results of the t-test analysis between GBF1 co-expressed with Arf1 and GBF1 co-expressed with Arf1/T31N. Blue corresponds to the results of the t-test analysis between GBF1 co-expressed with Arf1 and GBF1/E794K co-expressed with Arf1. Green corresponds to the results of the t-test analysis between GBF1 co-expressed with Arf1 and GBF1/7A co-expressed with Arf1. Yellow corresponds to the results of the t-test analysis between GBF1 co-expressed with Arf1/T31N and GBF1/E794K co-expressed with Arf1. Dark gray corresponds to the results of the t-test analysis between GBF1 co-expressed with Arf1/T31N and GBF1/7A co-expressed with Arf1. Dark pink corresponds to the results of the t-test analysis between GBF1/E794K co-expressed with Arf1 and GBF1/7A co-expressed with Arf1. The top box shows the p-value and the bottom box demonstrates the level of significance. No asterisks are used for p-values greater than 5E-2, one asterisk (\*) is used for p-values less than 5E-2, two asterisks are used for p-values less than 5E-3, three asterisks are used for p-values less than 5E-4, and four asterisks indicate p-values less than 5E-5.



**Supplemental Table 3:** The table lists the mean  $\pm$  standard deviation (STD)  $t_{1/2}$  values for Arf1-mCherry constructs co-expressed with GFP-GBF1 constructs. P-values are calculated with a two-tailed t-test and using  $\alpha = 0.05$ . To reduce space, scientific notation (i.e.  $3 \times 10^{-5}$ ) is abbreviated with an E (i.e. 3E-5). With five experimental conditions, there are a total of ten p-values calculated. Each pair of comparisons is denoted by similar color. Light green corresponds to the results of the t-test analysis between Arf1 expressed alone and Arf1 co-expressed with GBF1. Light blue corresponds to the results of the t-test analysis between Arf1 expressed alone and Arf1/T31N co-expressed with GBF1. Tan corresponds to the results of the t-test analysis between Arf1 expressed alone and Arf1 co-expressed with GBF1/E794K. Light gray corresponds to the results of the t-test analysis between Arf1 expressed alone and Arf1 co-expressed with GBF1/7A. Light pink corresponds to the results of the t-test analysis between Arf1 co-expressed with GBF1 and Arf1/T31N co-expressed with GBF1. Blue corresponds to the results of the t-test analysis between Arf1 co-expressed with GBF1 and Arf1 co-expressed with GBF1/E794K. Green corresponds to the results of the t-test analysis between Arf1 co-expressed with GBF1 and Arf1 co-expressed with GBF1/7A. Yellow corresponds to the results of the t-test analysis between Arf1/T31N co-expressed with GBF1 and Arf1 co-expressed with GBF1/E794K. Dark gray corresponds to the results of the t-test analysis between Arf1/T31N co-expressed with GBF1 and Arf1 co-expressed with GBF1/7A. Dark pink corresponds to the results of the t-test analysis between Arf1 co-expressed with GBF1/E794K and Arf1 co-expressed with GBF1/7A. The top box shows the p-value and the bottom box demonstrates the level of significance. No asterisks are used for p-values greater than 5E-2, one asterisk (\*) is used for p-values less than 5E-2, two asterisks are used for p-values less than 5E-3, three asterisks are used for p-values less than 5E-4, and four asterisks indicate p-values less than 5E-5.